RESEARCH PAPER

Synthesis of New Polymeric Composite Materials Derived from 2,2-(1,6-Dioxohexane-1,6-diyl) Dihydrazinecarbothioamide

***Fatimah A. Hasheem, Hanaa G. Attiya, Ruwaidah S. Saeed, Muna S. Al-Rawi** **

Department of Chemistry, College of Education for Pure Science(Ibn Al-Haitham), University of Baghdad, Iraq

ARTICLE INFO

Article History:
Received 02 April 2025
Accepted 12 August 2025
Published 01 April 2026

Keywords:
Composite Materials
FESEM
Molecular Docking
Nanopolymers
TGA

ABSTRACT

In this study, a new class of polymeric nanocomposites was synthesized and characterized. One mole of dimethyl adipate and two moles of thiosemicarbazide in ethanol first reacted to form the compound [C1]. Compound [C1] then reacted with sodium hydroxide to produce compounds [C2]. Hydrazine hydrate reacted with compound [C2] to generate compound [C3]. Compound [C4] was synthesized from compound [C3] and maleic anhydride. A polymer [C5] is formed by the reaction of the compound [C4] with ammonium persulfate as an initiator. This polymer was then combined with nano: ZnNPs, AgNPs, SiNPs, or IONPs using a hotplate stirrer for 3 hours to produce nanocomposites [C6-C9]. FTIR, ^{1}H-NMR, and Field Emission Scanning Electron Microscope (FESEM) were among the spectral analysis techniques used to identify the synthesized compounds. Investigations were also conducted into the thermal properties of TGA and DSC. Molecular docking was studied to evaluate the prepared compounds' free energy (ΔG) and predict their binding status with the enzyme. Lastly, examine the biological activities of polymers and nanocomposites that were screened using *Bacillus cereus* and *Escherichia coli*, as well as their anti-cancer activity against the human liver cancer cell line HepG2, using the normal cell line WRL68 as a comparison. In conclusion, the encouraging anticancer activities of the newly prepared nanocomposites induce more preclinical examination to move to clinical use in due course.

How to cite this article
Hasheem F., Attiya H., Saeed R., Al-Rawi M. Synthesis of New Polymeric Composite Materials Derived from 2,2-(1,6-Dioxohexane-1,6-diyl) Dihydrazinecarbothioamide. J Nanostruct, 2026; 16(2):2016-2030. DOI: 10.22052/JNS.2026.02.048

INTRODUCTION

When metal had been warmed and ceramics were modeled, the industrial production of the first synthetic polymer signaled yet an additional change in the evolution of humanity. As a result, then, the development of polymers has jumped dramatically. It could be proposed that these materials are now used in all aspects of human endeavor. Human curiosity and inventiveness, along with performance and financial factors, led to the development of this new class of materials. Consequently, research on blends of synthetic and natural polymers with possible applications in biological materials and ecology has recently increased [1,2]. In the 1980s, systems consisting solely of a polymer matrix with support from fabric components or inorganic filler materials were called polymer composites [3]. The

* *Corresponding Author Email: mona.s.s@ihcoedu.uobaghdad.edu.iq*

composite substances are made up of two or more components, one of which may be in the matrix phase and the other may be in the form of a fiber or molecule [4-6]. Construction, mechanical, automotive, marine, biomedical, and aerospace industries have all shown significant benefits from the use of natural or synthetic fibers in composite materials [7,8]. Nanocomposite substances have much better structural, thermal, mechanical, and tribological parameters than many traditional materials, according to studies done over the past 20 years [9,10]. The matrix material, which also includes nanoscale-confirming elements, makes up the structure of nanocomposites. These elements may be fibers, particles, nanotubes, whiskers, or other comparable elements [11]. Polymer nanocomposites are used in many different industrial products, such as those used in the electronics, automotive, and aerospace industries, because of their remarkable thermal properties [12,13]. Additionally, it has been found that triazole heterocyclic structures can form a wide variety of weak nonbond interactions with biological systems' enzymes and receptors [14]. Scientists from a variety of fields of study, including agricultural, chemical, medicine, supramolecular, polymer, and materials sciences, have gravitated to triazole compounds owing to their fundamental properties, which have made them major chromophores with significant medical potential [15]. Antifungal, antibacterial, anti-inflammatory, antiviral, antitubercular, anticoagulant, antioxidant, antidiabetic, and anticancer drugs based on triazole are among the many therapeutic drugs available [16]. The objective of this study is to first synthesize novel nanocomposites from dimethyl adipate with (ZnNPs, AgNPs, SiNPs, or IONPs), via a green method to increase their potential medical uses and improving their thermal analysis of their nanocomposites and polymers.

MATERIALS AND METHODS

All of the chemicals were supplied by Merck and Aldrich. FTIR spectra have been obtained using the Shimadzu FTIR spectrophotometer (Ir prestige 21) as well as KBr discs on an 8400 s spectrophotometer. The performed proton nuclear magnetic resonance (^{1}H-NMR) spectra were reported in ppm. These spectra were produced by Tehran, Iran's Bruker Ultra Shield 500MHz Razi Laboratories. The Sharif University of Technology in Tehran, Iran, uses Linseis Origin with platinum assessment V1.0.89 for thermogravimetric analysis (TGA/DSC).

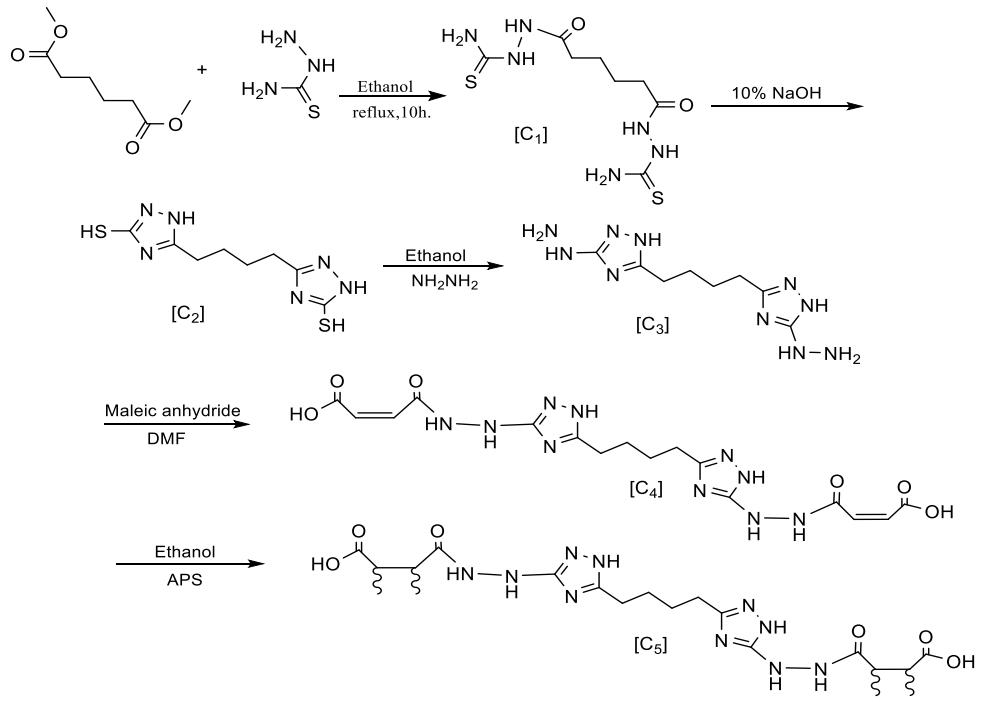

Fig. 1. illustrate all the steps to forming the newly compounds [C_1-C_5].

Synthetic Procedures

Figs. 1 and 2 illustrate the procedure to forming the newly nanocomposites.

Synthetic of 2,2'-(1,6-dioxohexane-1,6-diyl) dihydrazinecarbothioamide [C_1]

The initial compound was created by combining 0.87g and 0.01 mol of dimethyl adipate and 0.91g and 0.02 mol of thiosemicarbazide.10 ml of ethanol was then added, and the mixture was refluxed for ten hours before the excess solvent was removed [17]. White precipitate with a 93% yield, mp, 180–182°C.

Synthetic of 5-[4-(5-sulfanyl-1H-1,2,4-triazol-3-yl) butyl]-1H-1,2,4-triazole-3-thiol) [C_2]

After dissolving 0.73g,0.01mol of compound [C1] in 10 ml of 10% sodium hydroxide, the mixture was refluxed for a full day. Following the filtering step, the liquid was mixed with diluted hydrochloric acid to create an emulsion [18]. After filtering and washing the emulsion with water, we allowed the white precipitate to dry, yielding 78%, mp, 234–236°C.

Synthetic of 3-hydrazine-5-[4-(5-hydrazine-1H-1,2,4-triazole-3-yl) butyl]-1H-1,2,4-triazole [C_3]

5 ml of ethanol was used to dissolve 2.56 g,0.01mol of compound [C2]. Hydrozine hydrate (0.02 mol) was then added dropwise while stirring for 30 minutes [19], and the mixture was refluxed for 24 hours [20]. Following that, allow the sediment to dry to yield 72.5%, mp: 203-205°C.

Synthetic of fourth compound [C_4]

Compound [C3] (2.52 g, 0.01 mol) and maleic anhydride (1.96 g, 0.02 mol) were combined in 25 mL of DMF, and the mixture refluxed for approximately 4 hours. After using diethyl ether to clean the result, it was allowed to dry at room temperature [21]. m.p.: 175–177°C, yield 75%.

Synthetic of polymer [C_5]

0.42 g of ammonium persulfate and 0.41 g of the compound [C4] were mixed in 15 mL of ethanol as a polymerization initiator. After stirring

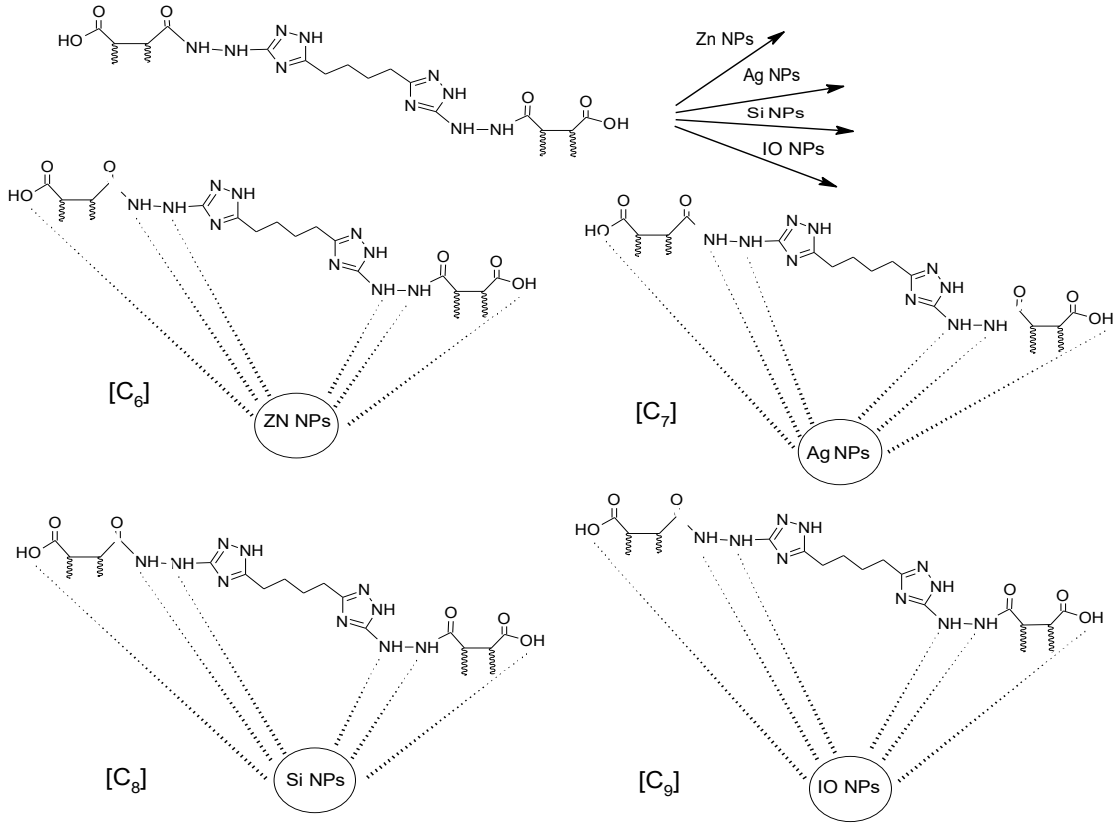

Fig. 2. Synthetic procedures of nanocomposites [C_6-C_9].

the mixture for two hours at room temperature, it refluxed for 12 hours [22]. 85% yield, m.p.: 260–262.

Synthetic of Nanocomposites [C_6-C_9]

50mL of a 250 mg/L solution of the nanoparticles [zinc nanoparticles (ZnNPs), silver nanoparticles (AgNPs), silica nanoparticles (SiNPs), or iron oxide nanoparticles (IONPs)] was combined with 100mg of dried polymer [C5] using a hotplate stirrer for three hours to bond the nano metal in the blend matrix [23].

Molecular Docking Study

The full Genetic Optimization of the British Cambridge Crystallographic Data Center (CCDC) (GOLD) Hermes 2021.2.0 (Build 327809) made it feasible to conduct molecular docking studies of compounds. This made it possible to show proteins, ligands, short contacts, hydrogen bonding interactions, and bond length computations. The effectiveness of the enzyme (6NE7) was shown

Table 1. FTIR of Compounds [C_1-C_9].

Com. no.	υ(NH_2)	υ (N-H)	υ(C-H) aliph	υ(C=O) amide	(C=N) & υ(C=C)	υ(Si-O)	υ(AgO)	υ(ZnO)	υ(FeO)
[C_1]	3357, 3255	3165	2953-2850	1641	-	-	-	-	-
[C_2]	-	3155	2922-2851	-	1636	-	-	-	-
[C_3]	3353	3175	2920-2851	-	1630	-	-	-	-
[C_4]	-	3110	2920-2848	1660	1620 1594	-	-	-	-
[C_5]	-	3185	2918-2850	1652	1630	-	-	-	-
[C_6]	-	3203	2924-2854	1680	1613	444	-	-	-
[C_7]	-	3188	2914-2852	1670	1625	-	439	-	-
[C_8]	-	3198	2924-2854	1660	1641	-	-	450	-
[C_9]		3197	2924-2854	1670	1624	-	-	-	443

Table 2. Molecular docking of compound [C_5].

Docking study (Antilungcancer)					
Compounds	*Binding Energy (PLP Fitness) Kcal/Mol*	*No. of Amino Acids Included in H-bonding*	*Amino Acids Included in H-bonding*	*no. of bonding*	*power of bonding*
6NE7	51.58	4	ARG770	2	2.855, 2.867
			VAL906	1	2.795
			TYR928	1	2.961
[C_5]	76.41	5	ARG770	2	2.943, 2.954
			VAL906	1	2.862
			ARG908	1	2.966
			SER909	1	2.761

using the Protein Data Bank (rcsb.org) [24].

Biological Activity

The cup-plate agar diffusion method was used to ascertain whether the nanocomposite, a polymer comprising zinc nanoparticles, silver nanoparticles, silica nanoparticles, and iron oxide nanoparticles, possesses antibacterial properties against *Escherichia coli* and *Bacillus cereus*. Amoxicillin, which was given at a concentration of 50µg/ml, was a common drug for antibacterial activity. After being sterilized, these agar solutions were placed in petri dishes and left to become solid. A micropipette has been used to sequentially introduce several of the synthesized compounds into the cavities. After that, these substances were given an hour to spread. All of the compounds have been dissolved in DMSO, which has also been used as a management. These plates were heated up for 24 hours at 37°C to test for antibacterial activity. The area of resistance surrounding the cups after the corresponding incubation was

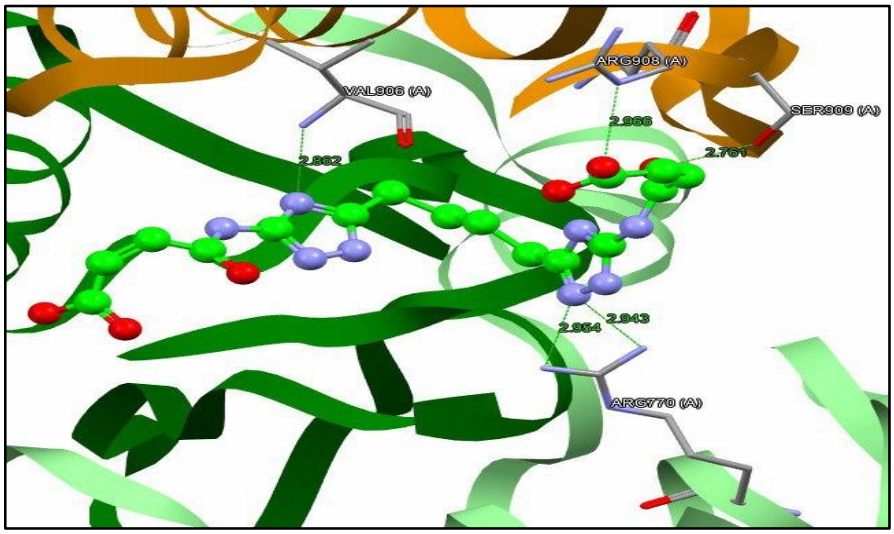

Fig. 3.Molecular docking of compound [C_5].

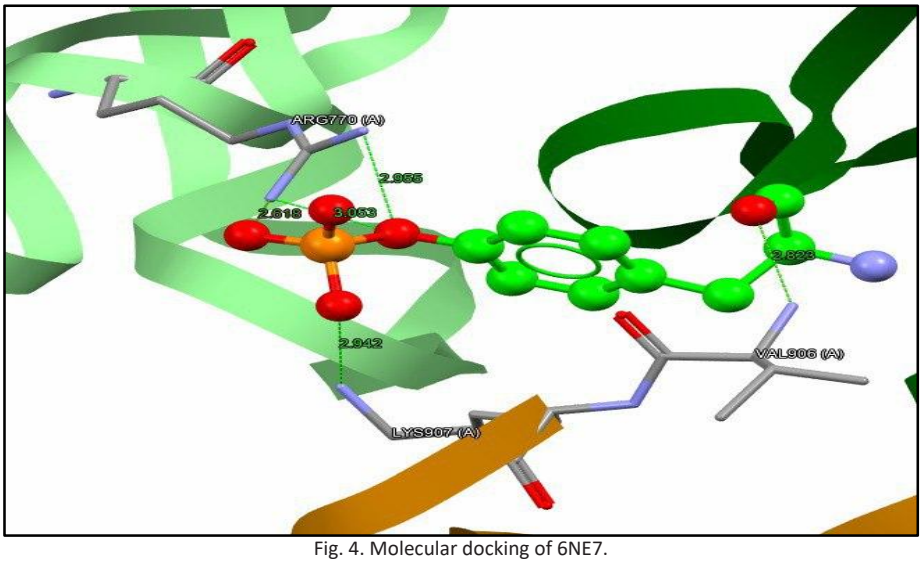

Fig. 4. Molecular docking of 6NE7.

measured in millimeters [25-27].

Cytotoxicity Activity

A human liver cancer cell line (HepG2) was used to test the cytotoxic impact of the polymer [C5] and nanocomposite [C6] (polymer and ZnNPs), and the outcomes were contrasted with those of a normal liver cell line (WRL-68). To investigate the cytotoxic effect, 96-well plates were used for the MTT test. Cells were treated with polymer [C5] and nanocomposite [C6] after 24 hours, or if a nanocomposite was created. Once the cells had been treated for twenty-four hours, the medium was removed, µl/well solutions of MTT were added, and the samples were incubated for four hours at 37°C to assess the viability of the cells. Afterward the removal of the MTT solution, 200µL of DMSO (Dimethyl Sulfoxide) was added to the wells to dissolve the crystals [28-30]. The mixture was then shaken frequently and incubated at 37 degrees Celsius for 15 minutes. The absorbency at a wavelength of 620 nm was measured using a microplate reader. Equations Freshney have been made available to calculate the rate of cell growth inhibition [31-33].

$$\text{Rate of Inhibition} = \frac{\text{mean of control} - \text{mean of treatment}}{\text{mean of control}} \times 100$$

RESULTS AND DISCUSSION

FTIR and ^{1}HNMR of synthesis of compounds

An overview of the reactions carried out in this investigation is given in Figs. 1 and 2. A new stretching band at 1641 cm^{-1} that was attributed to the C=O group of the amide moiety appeared in the FT-IR spectrum for compound [C1], replacing the absorption stretching band of the C=O groups ester in the starting materials. Many signals at δ (1.50-2.31) ppm for (m,4H, $CH_2CH_2CH_2CH_2$), multiple signals in the region δ (3.53-3.57) ppm for (m,4H, $CH_2CH_2CH_2CH_2$), at (4.30-4.48) ppm for (b,4H, NH_2), and a singlet signal at δ7·18 ppm for (s,2H, NH-C=S) were detected in the ^{1}H-NMR spectrum of compound [C1] (in DMSO-d_6 as solvent). Lastly, (s, 2H, NH-C=O) is responsible for a singlet signal at δ 7.54 ppm. When compound [C1] reacted with sodium hydroxide, compound [C2]

Table 3. Data of anti-bacterial screening of some of the synthesized polymers.

Comp.No.	Inhibition Zone (mm) of *E .coli*	Inhibition Zone (mm) of *Bacillus cereus*
Amoxicillin	17	23
[C_6]=polymer +ZnNPs	22	25
[C_7]= polymer +AgNPs	17	18
[C_8]= polymer +SiNPs	16	13
[C_9]= polymer +IONPs	25	22

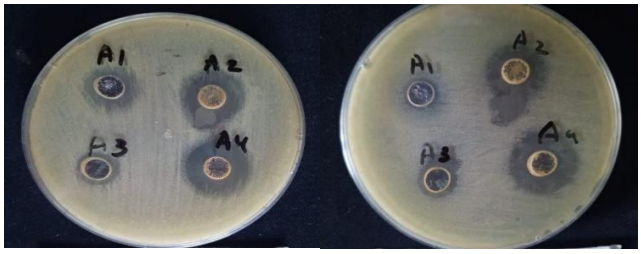

Fig. 5. Antibacterial activities of nanocomposities [C_6].

Table 4. IC50 of polymer [C_5] for HepG2andWRL-68.

Cell Line	IC_{50} µg mL^{-1}
HepG2	92.65
WRL-68	54.43

was created. The FTIR of compound [C2] revealed new absorption stretching bands at 2491 and 1313 cm^{-1}, which are allocated to the υ SH and υ C=S groups, respectively, and the disappearance bands

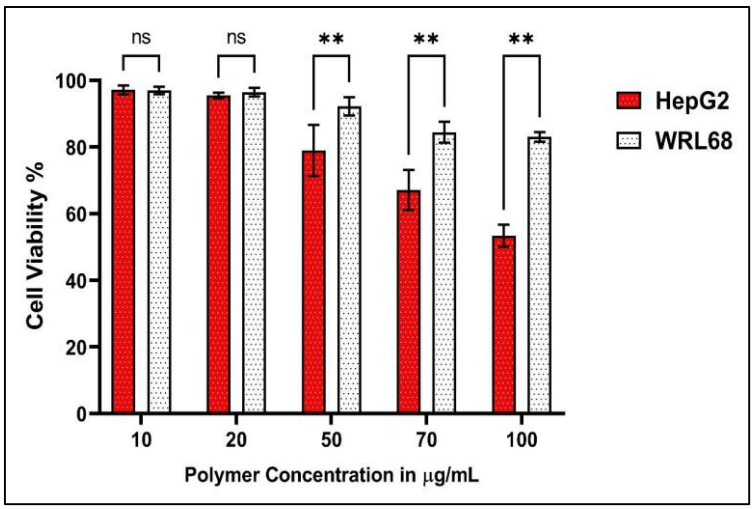

Fig. 6. Cell Viability of polymer [C_5] for HepG2 and compare with WRL68.

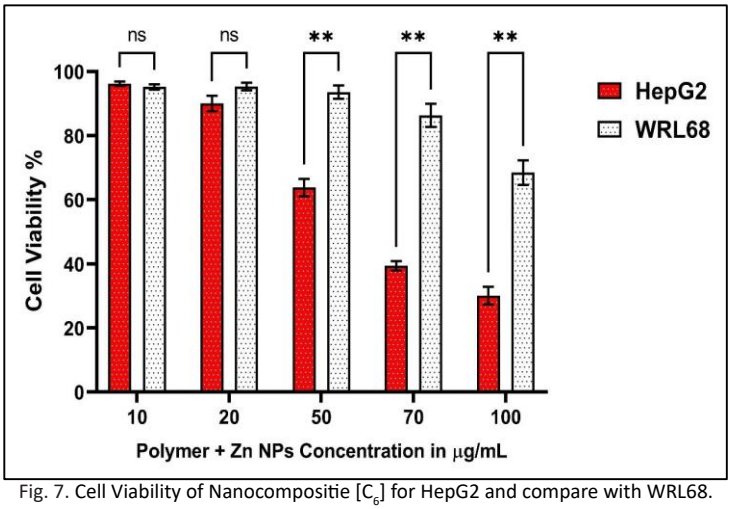

Fig. 7. Cell Viability of Nanocompositie [C_6] for HepG2 and compare with WRL68.

Table 5. Differences of polymer [C_5] between HepG2 and WRL68 with respect treatments.

	HepG2	WRL68	HepG2	WRL68
Concen.	Mean	Mean	SD	SD
10	97.15	96.95	1.35	1.14
20	95.45	96.49	0.88	1.29
50	78.97	92.21	7.66	2.78
70	67.09	84.45	6.09	3.12
100	53.40	83.06	3.31	1.45

of the NH_2 groups. Additionally, a stretching band for the 1,2,4-triazole ring's υ C=N (endocyclic) was seen at (1602-1636) cm^{-1}. The ^{1}H-NMR spectrum of compound [C2] revealed a singlet signal at 1.43 ppm for (s,2H, SH), numerous signals in the region (δ, ppm): (1.21-1.24) for (m,4H, $CH_2CH_2CH_2CH_2$), and signals (t,4H, $CH_2CH_2CH_2CH_2$) at (0.80-0.85). Finally, for (broad, 2H, NH) at (1.55.157) ppm [34-36]. One mole of compound [C2] was replaced neucleophilically with a sufficient amount of 80% hydrazine hydrate in absolute ethanol as a solvent to create the compound [C3]. The compound

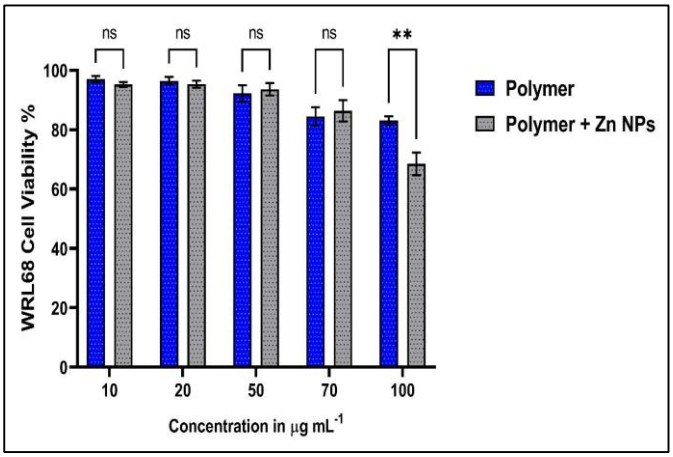

Fig. 8. Cell Viability of WRL68 for Polymer [C_5] and compare with polymer+ZnNPs [C_6].

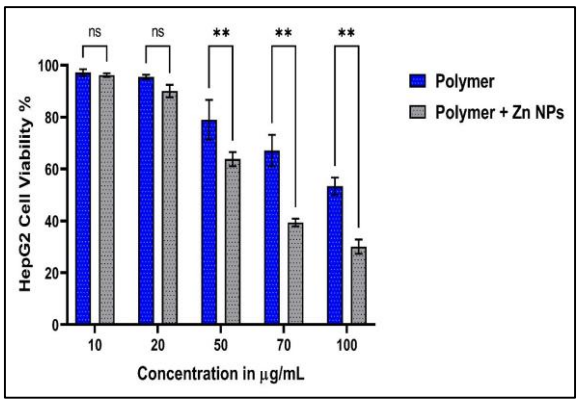

Fig. 9. Cell Viability of HePG2 for Polymer [C_5] and compare with polymer+ZnNPs [C_6].

Table 6. HepG2 and WRL68 Cells – Differences between polymers [C_5].

Šídák's multiple comparisons test HepG2 - WRL68	Below threshold	Summary	Adjusted P Value
10	No	Ns	>0.9999
20	No	Ns	0.9985
50	Yes	**	0.0012
70	Yes	**	<0.0001
100	Yes	**	<0.0001

[C3]'s FT-IR spectra revealed the emergence of new absorption stretching bands in the region (3300-3353) cm^{-1} and 3175cm^{-1}, which have been attributed to (NH_2, NH), respectively, along with the disappearance of absorption bands due to the (C=S) and (SH) groups. The compound [C3]'s ^{1}H-NMR spectrum revealed signals (t,4H, $CH_2CH_2CH_2CH_2$) at δ (0.78-0.86) ppm, numerous signals in the δ (1.30-1.33) ppm region for (m,4H, $CH_2CH_2CH_2CH_2$), a singlet signal at (1.19-130) ppm for (s,4 H, NH), and the (broad, 4H, NH_2) at (3.70-422) ppm. Compound [C4] was synthesized from compound [C3] and maleic anhydride. Because of the carboxylic acid's C=O, the compound [C4]'s

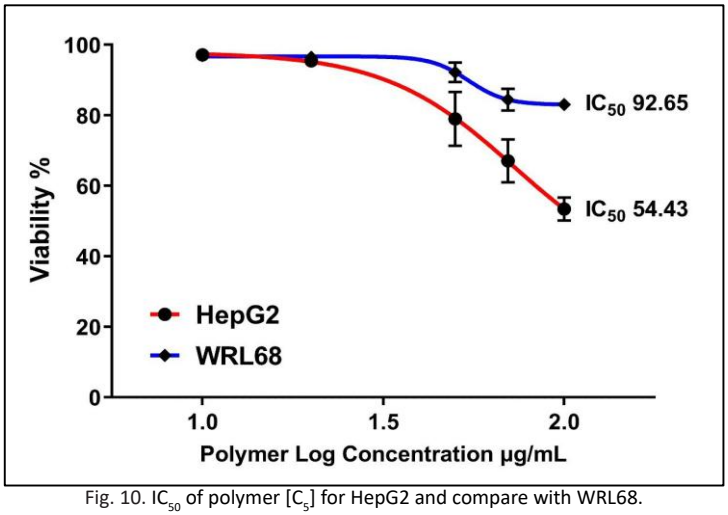

Fig. 10. IC_{50} of polymer [C_5] for HepG2 and compare with WRL68.

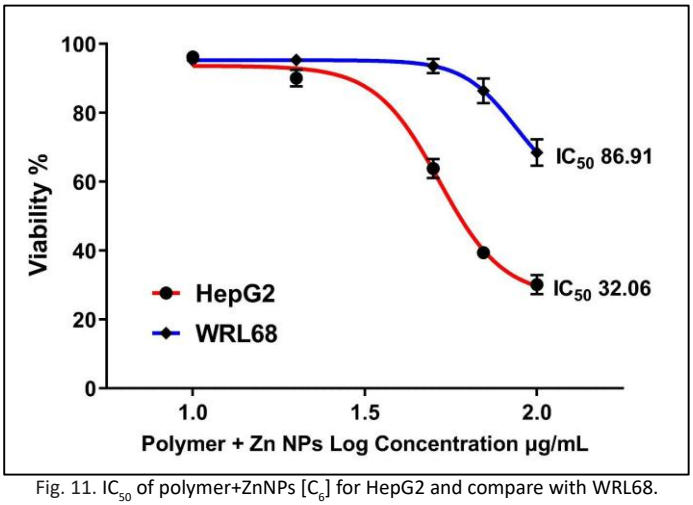

Fig. 11. IC_{50} of polymer+ZnNPs [C_6] for HepG2 and compare with WRL68.

Table 7. IC_{50} of Nanocomposite [C_6] for HepG2 andWRL-68.

Cell Line	IC_{50} µg mL^{-1}
HepG2	32.91
WRL-68	86.91

FTIR shows a new band at 1699 cm^{-1} and the disappearance of NH_2. Compound [C4] reacts with ammonium persulfate as an initiator to produce polymer [C5]. The FTIR of the polymer [C5] shows that the band at 1597 cm^{-1} is gone because of the υ C=C, Table 1. The ^{1}H-NMR spectrum of compound [C5] shows that there are many signals in the region δ (3.37-3.39) ppm for (m,4H, $CH_2CH_2CH_2CH_2$), a triplet signal at δ (3.7-3.8) ppm is due to (t,8 H. O= C-CH_2 –CH_2-C=O), a broad signal at δ (4.59-4.70) ppm for (broad,2H, NH of ring), and finally at (6.95-7.29) ppm for (2H, NH-C=O). This polymer was then combined with nano, which showed the bands at (439-450) cm^{-1} due to NPs bonding with the polymer [C5] [37,38].

Molecular Docking Study

The synthesized polymer [C5] showed notable activity in the examination of the stability of cancer cells in the enzyme (6NE7) due to hydrogen bond interactions with the primary amino acids ARG770, VAL906, and TYR928, [39] (Protein Data Bank, rcsb.org).

The prepared polymer [C5] Fig. 3 was more efficient and had a higher binding energy of 76.41 with the enzyme than the compound under comparison, Fig. 4, which had a binding energy of 51.58. This was because, as Table 2 shows, the compound was interacting with the primary amino acids ARG770, VAL906, ARG908, and SER909 through hydrogen bonds [40].

Biological activity

With the highest activity comparable to that of amoxicillin, the common antibiotic, the nanocomposites [C6-C9] Fig. 5 showed an extraordinary rate of inhibition against two pathogenic bacterial types *(G+) Bacillus cereus*

Table 8.Differences of Nano composite [C_6] between HepG2 and WRL68 with respect to treatments.

	HepG2		WRL68	
Concen.	Mean	SD	Mean	SD
10	96.22	0.68	95.22	0.82
20	90.05	2.42	95.33	1.18
50	63.81	2.74	93.60	2.10
70	39.39	1.46	86.34	3.61
100	30.09	2.77	68.48	3.82

Table 9. HepG2 and WRL68Cells – Differences between of Nanocomposite [C_6].

Šídák's multiple comparisons test HepG2 - WRL68	Below threshold	Summary	Adjusted P Value
10	No	Ns	0.9915
20	No	Ns	0.0680
50	Yes	**	< 0.0001
70	Yes	**	< 0.0001
100	Yes	**	< 0.0001

Table 10. HepG2- Cells – Differences between polymer and Nanocomposite [C_6].

Šídák's multiple comparisons test polymer and polymer – ZnNPs	Below threshold	Summary	Adjusted P Value
10	No	Ns	0.9992
20	No	Ns	0.3572
50	Yes	**	0.0003
70	Yes	**	<0.0001
100	Yes	**	<0.0001

and *E. coli (G–)*, Table 3. Because of their high cell affinity and ease of absorption by immune cells, NPs can be precisely delivered to the site of infection, where they can inhibit and harm microbiological pathogens. Since they strongly attach to electron donor groups—such as elements like sulfur, nitrogen, or oxygen—found in microbial cell walls and penetrate the bacterial cell wall, nanoparticles (NPs) have an antibacterial effect. Although they also release free radicals, NPs can harm cells and rupture their membranes [41-43]. Recent research suggests that magnetic nanoparticles could be harmful to microorganisms [44,45].

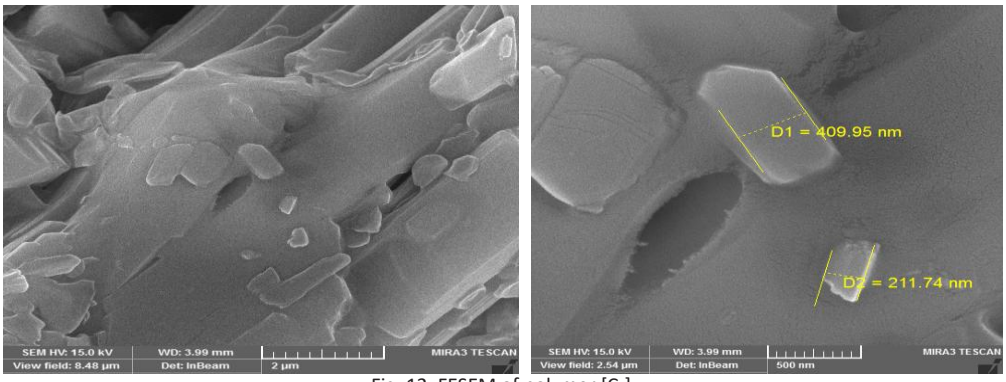

Fig. 12. FESEM of polymer [C_5].

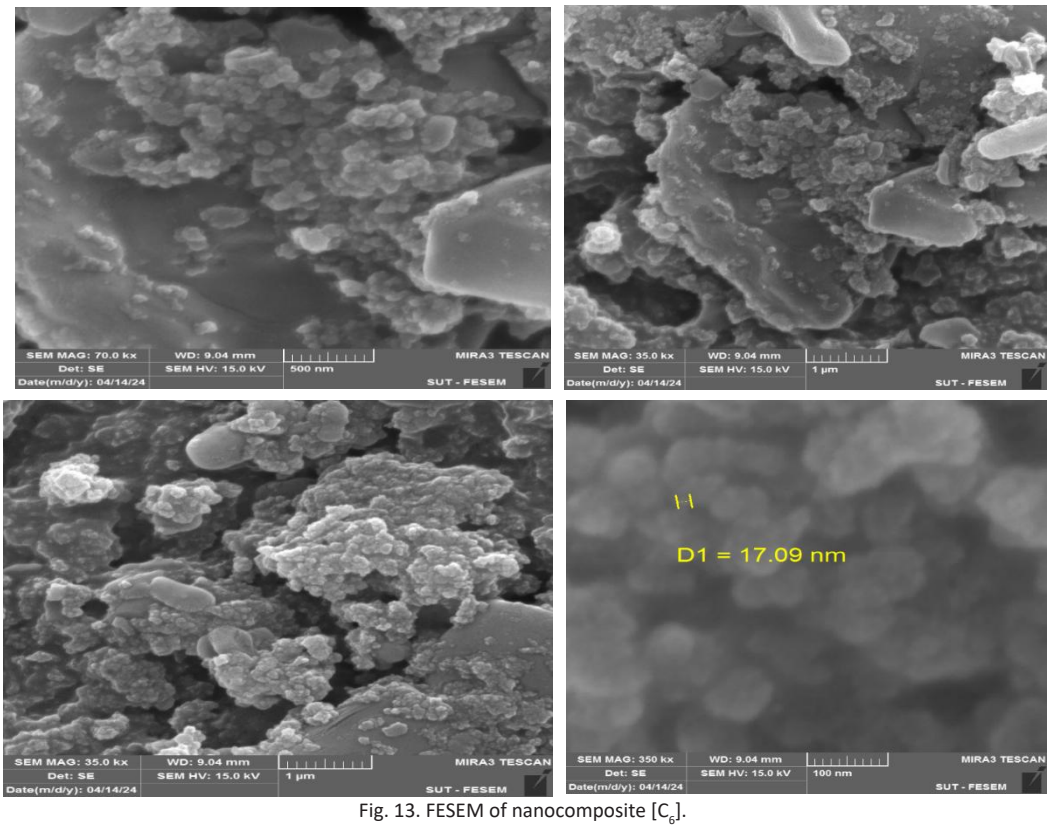

Fig. 13. FESEM of nanocomposite [C_6].

Cytotoxicity activity

The nanocomposite [C6] and polymer [C5] may be able to enter cancer cells specifically. At concentrations (10, 20, 50, 70, and 100) µg/ml higher than the polymer [C5], the nanocomposite [C6] demonstrated good inhibition, as indicated by Figs. 6- 11 and Tables 4-11. ZnNPs can induce cytotoxicity by increasing ROS levels [40]. One of the recent studies showed that they were effective cytotoxic agents when administered *in vivo*. It appears that magnetic ZnNPs mediate the DNA lesions in the tumor cells. Accordingly, at concentrations of 100 µg/ml, Nanocomposite [C6]'s anticancer activity showed significant effects against the HepG2 cell line, with an IC50 of 32.06 and an IC50 of 86.91 for (WRL-68) [46-48].

Field Emission Scanning electron microscope studies (FESEM)

The dimensions and shape of the polymer [5]

Table 11. WRL-68 Cells – Differences between polymer and Nanocomposite [C_6].

Šídák's multiple comparisons test polymer and polymer – ZnNPs	Below threshold	Summary	Adjusted P Value
10	No	Ns	0.9100
20	No	Ns	0.9831
50	No	Ns	0.9631
70	No	Ns	0.8769
100	Yes	**	<0.0001

NS: Non-significant; * p < 0.05; ** p < 0.01

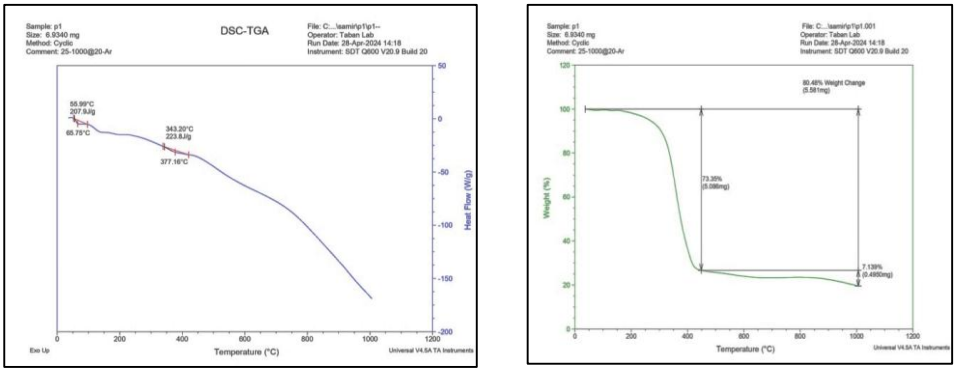

Fig. 14. DSC and TGA of the polymer [C_5].

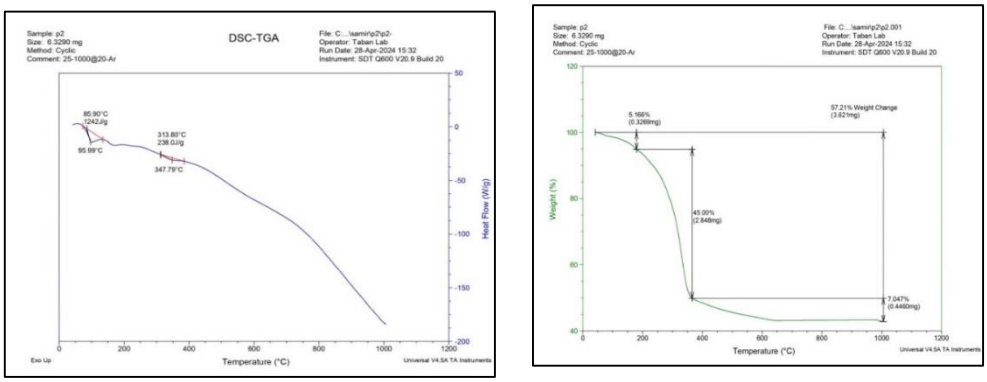

Fig. 15. DSC and TGA of nanocomposite [C_6].

and the nanocomposite [C6] have been approved using FESEM. The average size of the polymer [C5] Fig. 12 particles is between 211 and 409 nm. ZnNPs were found to be uniformly distributed across the matrix's surface; in the nanocomposite [C6] Fig. 13, their nanosize is 17.09 nm. However, when the surface is slightly difficult, some of the formation nanoparticles have also been found. According to several studies [49] the particles in nano-composite films have an almost spherical morphology.

Thermal analysis

For both pure polymers and novel nano-composites, thermo-gravimetric (DSC/TG) curves have been developed at a heating rate of 10 °C min^{-1} under argon. The temperature ranging from 0°C to 1200°C has been recorded. The thermal breakdown of pure polymer [C5] and nano-composite [C6] is shown in the table. The TGA curves of the polymer [C5] in Fig. 14 demonstrated two primary phases of weight loss. At a temperature of 45–450 °C, the first stage, which involved the evaporation of volatile compounds, primarily water, resulted in weight losses of roughly 73.35 %. At temperatures between 450 and 1020 °C, the polymer main chain disintegrated in the last one, resulting in weight losses of roughly -7.139 %. The polymer film DSC curve displays a glass transition temperature (TG) of (55.99) °C, an exothermic peak (130 °C) that represents the crystalline temperature Tc, and a sizable endothermic peak (Tm) at (377) °C that is associated with the melting of polymers.

The degradation of polymer (Td) begins at (470) °C. Fig. 15 depicts the nano-composite [C6] TGA thermo-gram, which reveals three stages of decomposition [49,50]. The weight loss from the first occurs between 45 and 200°C and is about 5.166%. The weight loss from the second occurs between 200 and 370°C and is about -45%; and the weight loss from the third occurs between 370 and 1010°C and is about 7.047. The DSC curve shows a degradation point at 550°C, an endothermic melting point (Tm) of 397°C for modified PVA, an exothermic peak at 85.90°C representing the glass transition temperature (Tg), and a crystalline temperature point (Tc) of 170°C [51,52].

CONCLUSION

Molecular docking, antibacterial and anticancer properties, field emission scanning electron microscopy, and thermal analysis of a few novel nanocomposites are all included in this study. The prepared polymer is more effective than the contrasting compound, according to the molecular docking study. Depending on the results, the development inhibition zone was wider for nanocomposites, and nanocomposites [C6] demonstrated outstanding antimicrobial activity against *Bacillus cereus* and *E. coli* that was comparable to that of amoxicillin, a common antibiotic. The anticancer activity of polymer [C5] and nanocomposites [C6] against HepG2 (a human liver cancer cell line) and normal cell line WRL68 (a normal liver cell line) was then examined. With IC_{50} values of 32.06 on HepG2 and 86.91 on WRL-68 cancer cell lines, nanocomposite [C6] demonstrated a high rate of restriction and reduced toxicity. The new bonds between the polymers and nanoparticles caused the surface morphology of the synthesized nanocomposites to change, as demonstrated by FESEM studies. Lastly, the findings showed that the prepared polymer [C5] is less thermally stable than the nanocomposite [C6].

CONFLICT OF INTEREST

The authors declare that there is no conflict of interests regarding the publication of this manuscript.

REFERENCE

1. Lakhdar Y, Tuck C, Binner J, Terry A, Goodridge R. Additive manufacturing of advanced ceramic materials. Prog Mater Sci. 2021;116:100736.
2. S. Saeed R, A. Hassan H, F. Hassan D, S. Al-rawi M. Modification and Study Biological Activity of Chitosan with Compounds Containing Azo Group. Baghdad Science Journal. 2024.
3. Kangishwar S, Radhika N, Sheik AA, Chavali A, Hariharan S. A comprehensive review on polymer matrix composites: material selection, fabrication, and application. Polym Bull. 2022;80(1):47-87.
4. Flower HM. An Introduction to Composite Materials — Second edition D. Hull and T.W. Clyne Cambridge University Press, The Pitt Building, Trumpington Street, Cambridge CB2 IRP. 1996. 326pp. Illustrated. £19.95. The Aeronautical Journal. 1997;101(1005):228-228.
5. Zagho M, Hussein E, Elzatahry A. Recent Overviews in Functional Polymer Composites for Biomedical Applications. Polymers. 2018;10(7):739.
6. Neves Monteiro S, Salgado de Assis F, Ferreira C, Tonini Simonassi N, Pondé Weber R, Souza Oliveira M, et al. Fique Fabric: A Promising Reinforcement for Polymer Composites. Polymers. 2018;10(3):246.
7. Movahedi N, Linul E. Quasi-static compressive behavior of the ex-situ aluminum-alloy foam-filled tubes under elevated temperature conditions. Mater Lett. 2017;206:182-184.
8. Linul E, Vălean C, Linul P-A. Compressive Behavior of Aluminum Microfibers Reinforced Semi-Rigid Polyurethane

Foams. Polymers. 2018;10(12):1298.
9. Chukov D, Nematulloev S, Torokhov V, Stepashkin A, Sherif G, Tcherdyntsev V. Effect of carbon fiber surface modification on their interfacial interaction with polysulfone. Results in Physics. 2019;15:102634.
10. Du Y, Li D, Liu L, Gai G. Recent Achievements of Self-Healing Graphene/Polymer Composites. Polymers. 2018;10(2):114.
11. Awaji H, Choi S-M. Toughening and Strengthening Mechanisms in Nanocomposites Based on Dislocation Activity. Fracture Mechanics of Ceramics: Springer US; 2005. p. 191-201.
12. Rahman MM, Khan KH, Parvez MMH, Irizarry N, Uddin MN. Polymer Nanocomposites with Optimized Nanoparticle Dispersion and Enhanced Functionalities for Industrial Applications. Processes. 2025;13(4):994.
13. Moisala A, Li Q, Kinloch IA, Windle AH. Thermal and electrical conductivity of single- and multi-walled carbon nanotube-epoxy composites. Composites Science and Technology. 2006;66(10):1285-1288.
14. Hitchcock CA, Dickinson K, Brown SB, Evans EGV, Adams DJ. Interaction of azole antifungal antibiotics with cytochrome P-450-dependent 14α-sterol demethylase purified from Candida albicans. Biochemical Journal. 1990;266(2):475-480.
15. H. Zhou C, Wang Y. Recent Researches in Triazole Compounds as Medicinal Drugs. Curr Med Chem. 2012;19(2):239-280.
16. Kumar S, Khokra SL, Yadav A. Triazole analogues as potential pharmacological agents: a brief review. Future Journal of Pharmaceutical Sciences. 2021;7(1).
17. Saroha M, Khurana JM. Acetic acid mediated regioselective synthesis of 2,4,5-trisubstituted thiazoles by a domino multicomponent reaction. New J Chem. 2019;43(22):8644-8650.
18. Gomha SM, Riyadh SM. Synthesis under Microwave Irradiation of [1,2,4]Triazolo[3,4-b] [1,3,4]thiadiazoles and Other Diazoles Bearing Indole Moieties and Their Antimicrobial Evaluation. Molecules. 2011;16(10):8244-8256.
19. Saeed RS. Synthesis and Characterization of O-(carboxyl) Chitosan Schiff Base Derivatives and Study Antibacterial Activity. International Journal of Drug Delivery Technology. 2020;10(03):402-407.
20. Novel Azo Compounds Derived from Thiazolidine-4-one: Synthesis, Metal Complexation, Coloristic Properties, and Biological Activity. American Chemical Society (ACS).
21. Attiya HG, Saeed RS, Hasheem FA, Al-Rawi MS. Synthesis of Few New Carrier Polymers Derived from 2-hydrazinylbenzo[d]thiazole. International Journal of Drug Delivery Technology. 2022;12(04):1792-1796.
22. Li X, Huang Y, Dan Y. Synthesis of sub-100 nm PMMA nanoparticles initiated by ammonium persulfate/ascorbic acid in acetone-water mixture. Colloid Polym Sci. 2020;298(3):225-232.
23. Saeed RS, Attiya HG, Obead KA. Synthesis and Characterization of Grafted Chitosan Blending with Polyvinyl alcohol / Nanocomposite and Study Biological Activity. Baghdad Science Journal. 2023.
24. Özcan H. Pyrrole-Based Schiff-Bases: Synthesis, Fluorescent Properties, Molecular Docking and in silico ADME/Tox Profiling Studies. ChemistrySelect. 2023;8(11).
25. Tomma JH, Al-Obaidi OB, Al-Dujaili AH. A new thiazoldinone and triazole derivatives: Synthesis, characterization and liquid crystalline properties. J Mol Struct. 2022;1270:133817.
26. Study the Toxicity and Anticancer activity of Some New Amic Acid and Their Derivatives of Mefenamic acid. Indian Journal of Forensic Medicine and Toxicology. 2020.
27. Rumez RM, Abdul-Razaq AaS, Hassan DF, Hussin ZH. Synthesis and Biological Activity Study of New Some Schiff Bases Derived From D-Erythroascorbic Acid. Journal of Al-Nahrain University Science. 2017;17(2):46-54.
28. Ali M, Drea AAA. Green synthesis of nano binary oxide SiO_2/V_2O_5 NPs integrated ointment cream application on wound dressings and skin cancer cells. Baghdad Science Journal. 2023;20(3):0734.
29. S. Al-Rawi M, A. Hassan H, F. Hassan D, Y. Majeed I. New Series of Substituted Heterocyclics Derived from α , β – Unsaturated Ketone and Their Cytotoxic Activity Tumor Cell Lines. Oriental Journal of Chemistry. 2018;34(6):2826-2831.
30. Hasan AM, Majeed SMA. Detection of Anti-cancer Activity of Silver Nanoparticles Synthesized using Aqueous Mushroom Extract of Pleurotus ostreatus on MCF-7 Human Breast Cancer Cell Line. Iraqi Journal of Science. 2024:1886-1894.
31. The Cytotoxic Effect of Zno Nps Against the Intracellular Amastigotes of Leishmania Donovani in Vitro. Iraqi Journal of Science. 2017;58(4C).
32. Gao S. Antiproliferative effect of octreotide on gastric cancer cells mediated by inhibition of Akt/PKB and telomerase. World J Gastroenterol. 2003;9(10):2362.
33. Freshney RI. Culture of Animal Cells: Wiley; 2010 2010/09/20.
34. Ikhlas Hassan Budaiwi S, Ahmed R. Cognitive Excavation in the Sufi Terminology of Nazla Al-Jubouri. Journal of Namibian Studies : History Politics Culture. 2023;33.
35. Yousefi M, Khanniri E, Sohrabvandi S, Khorshidian N, Mortazavian AM. Encapsulation of Heracleum persicum essential oil in chitosan nanoparticles and its application in yogurt. Frontiers in Nutrition. 2023;10.
36. Synthesis, Characterization, Study the Toxicity and Anticancer Activity of N,O-Chitosan Derivatives. International Journal of Pharmaceutical Research. 2020;12(02).
37. Alheety KA, Jamel NM, Hameed WMA-A, Al-Rawi MS, Tomma JH. Synthesis and Study of the Biological Activity of New Compounds Derived from 4-(5-Phenyl-1,3,4-oxadiazole-2-yl)aniline. Russ J Org Chem. 2024;60(7):1342-1347.
38. Noori Abdullah M. Synthesis, Antimicrobial, Antioxidant Evaluation, and DFT Estimation of some New Cyclohexenone Derivatives Derived from Benzyloxy Chalcones. Current Organic Synthesis. 2023;20(7):812-820.
39. Al-kadhimi A, Muhsin MK, Al-Salami MAJ. Synthesis and Characterization of Some Schiff Bases Derived from Carboxymethyl Chitosan and Evaluating The Biological Activity of Some of these Derivatives. Kirkuk University Journal-Scientific Studies. 2021;15(4):56-86.
40. Devi JS. Anticancer Activity of Silver Nanoparticles Synthesized by the Seaweed Ulva lactuca Invitro. Journal of Nanomedicine and Biotherapeutic Discovery. 2012;02(03).
41. Armijo LM, Wawrzyniec SJ, Kopciuch M, Brandt YI, Rivera AC, Withers NJ, et al. Antibacterial activity of iron oxide, iron nitride, and tobramycin conjugated nanoparticles against Pseudomonas aeruginosa biofilms. Journal of Nanobiotechnology. 2020;18(1).
42. Vallabani NVS, Vinu A, Singh S, Karakoti A. Tuning the ATP-triggered pro-oxidant activity of iron oxide-based nanozyme towards an efficient antibacterial strategy. Journal of Colloid

and Interface Science. 2020;567:154-164.
43. Shareef AA, Hassan ZA, Kadhim MA, Al-Mussawi AA. Antibacterial Activity of Silver Nanoparticles Synthesized by Aqueous Extract of Carthamus oxycantha M.Bieb. Against Antibiotics Resistant Bacteria. Baghdad Science Journal. 2022;19(3):0460.
44. Saeed RS, Hussein FA, Awad SH, Al-rawi MS. Synthesis and Study Antibacterial Activity of Some New Polymers Containing Maleimide Group. Journal of Physics: Conference Series. 2021;1879(2):022070.
45. Synthesis and Study the Biological Activity of New Heterocyclic Compounds Derived From Hydrazide Derivatives. Indian Journal of Forensic Medicine and Toxicology. 2020.
46. Jantas R, Draczyński Z, Herczyńska L, Stawski D. Poly(vinyl alcohol)-Salicylic Acid Conjugate: Synthesis and Characterization. American Journal of Polymer Science. 2012;2(5):79-84.
47. Haghighi P, Ziyadi H, Hekmati M, Habibnejad N, Iranfar S. Hibiscus sabdariffa extract/poly (vinyl alcohol) modified magnetite as a magnetically recyclable nanocatalyst for the selective oxidation of amines. Results in Chemistry. 2022;4:100483.
48. Ali Ia. Characterization of Zinc oxide Nanostructures prepared by hydrothermal method with Antibacterial property. Iraqi Journal of Physics. 2019;17(42):108-124.
49. Abed Al, Hussein MT. Synthesis and Characterization of Ternary $Be_xZn_{1-x}O$ Nano Thin Films prepared by Pulsed Laser Deposition Technique. Iraqi Journal of Physics (IJP). 2022;20(2):53-63.
50. Effect of silver nanoparticles on macrophage cytotoxicity upon exposure to Leishmania tropica in vitro. Iraqi Journal of Science. 2017;58(3B).
51. Hameed TM. A study of the effect of nano materials on the physical properties of epoxy composites. Iraqi Journal of Physics. 2019;15(32):68-76.